Journal of Materials Chemistry C

Accepted Manuscript

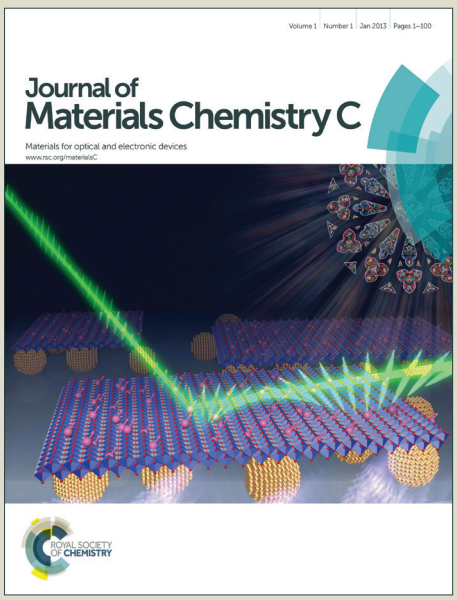

ROYAL SOCIETY OF CHEMISTRY

www.rsc.org/materialsC

Cite this: DOI: 10.1039/c0xx00000x

www.rsc.org/xxxxxx

FULL PAPER

β Phase PVDF-*hfp* Induced by Mesoporous SiO_2 Nanorods: Synthesis and Formation Mechanism

Du Yuan,[a] Zibiao Li,[b] Warintorn Thitsartarn,[b] Xiaoshan Fan,[a] Jiaotong Sun,[a] Hui Li[a] and Chaobin He*[a,b]

Received (in XXX, XXX) Xth XXXXXXXXX 20XX, Accepted Xth XXXXXXXXX 20XX
DOI: 10.1039/b000000x

Poly(vinylidene fluoride) (PVDF) homopolymer and its copolymers in their *β* phases are the most promising polymeric materials for electroactive devices. In this work, a simple and effective strategy is developed to fabricate *β*-Poly(vinylidene fluoride-co-hexafluoropropylene) (*β*-PVDF-*hfp*) with its characteristic piezo-/ferro-electric properties using mesoporous SiO_2 nanorods. The nanorods offer 2-fold arrangement for the –OH groups, namely, anisotropic rod shape and ordered mesopores. We report, for the first time in the PVDF system, the direct evidence on hydrogen bond interaction during *β* phase formation through XPS analysis. Our study further reveals that besides well-known facilitation by intermolecular interaction, the arrangement of surface functional groups is essential for the formation of *β*-PVDF-*hfp*. This proposed mechanism manages to explain current controversy in the formation mechanism. We further demonstrates that our approach can be extended towards wider intermolecular interaction regime than hydrogen bonding, thus benefitting current development in PVDF homo/copolymer-based electroactive devices.

Introduction

As one of the most important polymeric electroactive materials, poly(vinylidene fluoride) (PVDF) homopolymer and its copolymers with pyro-/ferro-/piezo-electric properties have obtained wide applications including acoustic transducers, infrared detector, piezoelectric sensors, information storage memory, and currently developed flexible and stretchable energy harvesting systems.[1-7] Within the five reported crystalline phases of PVDF (denoted as *α*, *β*, *γ*, *δ*, *ε*), the all-trans polar *β* phase with the largest spontaneous polarization per unit cell presents the superior properties.[1,8-10]

It remains still a great challenge to develop efficient and reliable methods for entire formation of *β* phase in PVDF and its copolymer (like Poly(vinylidene fluoride-co-hexafluoropropylene) (PVDF-*hfp*)) against the thermodynamically stable nonpolar *α* phase. Numerous endeavors include mechanical stretching via forced molecular conformation, electric poling through aligning the crystalline polar axis, electrospinning, low-temperature polar solvent crystallization, addition of nucleation agents/surface charged nucleation agents, addition of nanofiller (e.g., carbon nanotube (CNT), $BaTiO_3$, and $CoFe_2O_4$), and recently developed template methods (e.g., anodized alumina memebrane).[11-24] It is well known that intermolecular bonding from diverse molecules or surface functional groups promotes the *β* phase formation of PVDF and its copolymers. Polar interaction between PVDF and polar solvents (e.g., dimethylformamide, dimethylacetamide) leads to polar phase formation through crystallization during solvent evaporation.[15] Recent study reveals the incorporation of positive charged organic molecules/nucleating agents facilitate the formation of polar phases (*β*, *γ*) via positive ion-CF_2 dipole.[17] The surface nature of nanofillers on the formation of polar phases has been investigated, e.g., the effects of interfacial bonding between surface modified single-wall/multi-wall carbon nanotubes and ion-dipole interaction between ionic surfactant modified $CoFe_2O_4$.[18-21] Moreover, the application of the templates permits a confinement effect on the growth of *β*-PVDF nanowires with preferential molecular orientation.[22-24] The proposed formation mechanism is attributed to the hydrogen bonding between hydroxyl groups (–OH) and carbonfluroine (–CF), based on red-shift of the vibrational frequency of –OH via infrared spectroscopy.[23,25] Note that this spectroscopic feature is typically broad that details are hard to be uncovered. As discussed above, in order to achieve the thermodynamically unfavorable polar phase, an anchoring intermolecular interaction is necessary to overcome the conformation energy barrier. However, controversy apparently exists that the incorporation of SiO_2 nanoparticles with abundant –OH groups did not favor the growth of *β* phase.[26,27] This fact indicates underlying factor other than the intermolecular interaction for *β* phase formation. Inspired by the smart confinement method through templates, we hypothesize that the origin of *β* phase formation is 2-fold: (1) exsitence of a strong molecular interaction between fillers and PVDF matrix and (2) a long range arrangement of surface functional groups that anchor the interaction.

Herein, we report a simple and effective strategy to fabricate *β*-PVDF-*hfp* film by using mesoporous SiO_2 (*m*-SiO_2) nanorods. In this design, the *m*-SiO_2 nanorods offer 2-fold arrangement for the

–OH groups, namely, anisotropic rod shape and ordered mesopores. Impressively, entire β phase of PVDF-*hfp* with its characteristic structural properties and piezo-/ferro-electric performance can be achieved. In our study, direct and unambiguous evidence on the formation mechanism of β phase by hydrogen bond is provided through XPS analysis, which to the best of our knowledge is the first report in the PVDF system. Based on the effects of variuos types of SiO_2 nanostructures on β phase formation, we propose the essence of arrangement of surface functional groups/charges in influencing the formation of PVDF-*hfp*. We further demonstratate that other intermocular interaction regime could also be used to anchor the formation of β-PVDF-*hfp*.

Experimental

Materials Synthesis

The synthetic strategy of β phase *m*-SiO_2 nanorod@PVDF-*hfp* is presented in Fig. 1a. *m*-SiO_2 nanorods with a size of 276×133 nm (aspect ratio of ~ 2.1) were prepared based on a well-established soft-template method (Fig. 1b), where washing process was applied to endow them with –OH groups (Figure S1).[28,29] A simple film casting approach was applied on a homogeneous mixture of *m*-SiO_2 nanorods and PVDF-*hfp*/DMF solution under an elevated temperature with adjusted vacuum level to obtain the *m*-SiO_2 nanorod@PVDF-*hfp* nanocomposites.

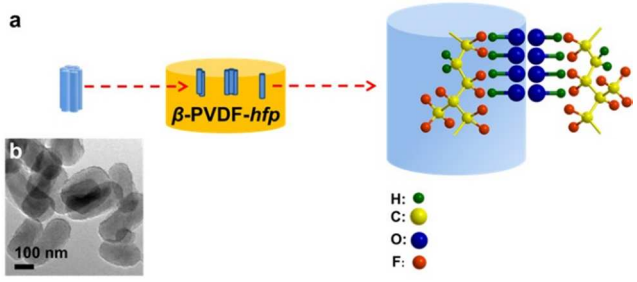

Fig. 1 (a) Schematic illustration of formation of β-PVDF-*hfp* by (b) *m*-SiO_2 nanorods.

In a typical synthesis of *m*-SiO_2 nanorods, cetyl trimethylammonium bromide aqueous solution (5 mg/mL, 25 mL) was first prepared, which was then heated to 50 °C in an oil bath followed by addition of ammonia (1.75 mL) and tetraethyl orthosilicate (1 mL). The mixture was aged with mild stirring for 24 h. As-synthesized samples were collected by centrifugation and washed with deionized H_2O and ethanol for at least 3 times. The template removal was performed by refluxing the as-synthesized samples in an acidic ethanol (1 mL concentrated HCl (37%) in 20 mL ethanol) for 6 h. Meanwhile, both of their exterior and interior surfaces were enriched with –OH groups (Figure S1). The *m*-SiO_2 nanorods were collected by further centrifugation and washing in ethanol and vacuum drying.

PVDF-*hfp* ($(-CF_2CH_2-)_{1-x}(-CF_2CFCF_3-)_x$, x=0.1, 1 g) was dissolved in dimethylformamide (DMF, 20 mL) at 50 °C for 4 h. The mixture of certain amounts of *m*-SiO_2 nanorods and PVDF-*hfp*/DMF solution was under ultrasonication (37 KHz) for 30 mins. The mixture was then put in a 50 °C oven with adjusted vacuum level (0.2 bar) for 24 h to form the *m*-SiO_2 nanorod@PVDF-*hfp* nanocomposite film.

Materials Characterizations

Fourier transform infrared spectroscopy-attenuated total reflectance (FTIR-ATR) spectra were collected by IR-Tracer 100 spectrometer (Shimadzu) with ATR ZnSe accessory with 128 scans and anominal resolution of 1 cm^{-1}. Powder X-ray diffraction (XRD) patterns were recorded by the D8 ADVANCE powder diffractometer (Bruker AXS Inc., Madison, WI) using λ_{Cu} K_α of 1.541 Å operated at 40 kV and 40 mA with a step size of 0.004°and step duration of 1 s. Small-angle/Wide-angle X-ray scattering (SAXS/WAXS) study was performed by Xeuss C HP200-fm (Xecuss SA) with ultralow divergence Cu K_α source with a simultaneous WAXS module. Differential scanning calorimetry (DSC, TA instrument Q100) analysis was performed under N_2 following the protocol: equilibrate at 25 °C, ramp 5 °C/min to 200 °C. Thermogravimetric analysis (TGA) spectra were obtained by heating the samples at a ramp rate of 10 °C/min to 850 °C. The morphology and microstructure of the synthesized *m*-SiO_2 nanorods and *m*-SiO_2 nanorod@PVDF-*hfp* were characterized by field emission scanning electron microscopy (FESEM, Zeiss) and transmission electron microscopy (TEM, JEOL 2010). The TEM sample for *m*-SiO_2 nanorod@PVDF-*hfp* was prepared by depositing a drop of *m*-SiO_2 nanorod@ PVDF-*hfp*/DMF solution onto a carbon-coated grid undergoing the identical vacuum and temperature condition for the film preparation. X-ray photoelectron spectroscopy (XPS) analysis was conducted using a Kratos Axis Ultra X-ray photoelectron spectroscopy (Kratos Analytical) with a momochromated Al K_α source (1486.5 eV) under the chamber pressure of 10^{-9} torr, where the elemental scans were based on 20 meV pass energy.

Piezo-/ferro-electric Performance

The *m*-SiO_2 nanorods and PVDF-*hfp*/DMF solution was casted on ITO substrate with identical film formation condition, followed by deposition of Au electrodes. The polarization-electric field hysteresis loops were measured by radiant precision workstation (Radiant Technologies, INC). The applied voltage was varied from 2 to 6 V with the frequency fixed at 2 ms. The piezoresponse force microscopy (PFM) phase image was obtained by MFP-3D AFM system (Asylum Research) with Pt/Ti coated tips. Contact mode was used with an AC voltage applied to the probe tip. The scan rate is kept at 0.5 m/s.

Results and discussion

Crystal and lamellar structure

FTIR-ATR spectra in Fig. 2a show that the 17.2 wt% *m*-SiO_2 nanorod@PVDF-*hfp* presented unambiguously the spectroscopic feature of β phase at 836 cm^{-1} ($-CH_2$ rocking), where the features of α phase at 615 cm^{-1} (skeletal bending), 763 cm^{-1} ($-CF_2$ bending), 797 cm^{-1} ($-CH_2$ rocking), and 976 cm^{-1} (twisting) as in the PVDF-*hfp* were not traced.[10,12,16] WAXS spectra show clearly the $\alpha \rightarrow \beta$ phase transformation in Fig. 2c. Though the PVDF-*hfp* reference showed coexisting α(100)(110) and (021) diffraction peaks and β(200)(110) peaks, the addition of *m*-SiO_2 nanorods into PVDF-*hfp* led to only the characteristic β(200)(110) peaks present.[15,23] Besides, a single endothermic peak in *m*-SiO_2 nanorod@PVDF-*hfp* was observed by DSC comparing to bimodal peaks in the PVDF-*hfp* (Fig. S2). The consistency in

above analysis verifies the entire formation of β-PVDF-*hfp* by *m*-SiO_2 nanorods.

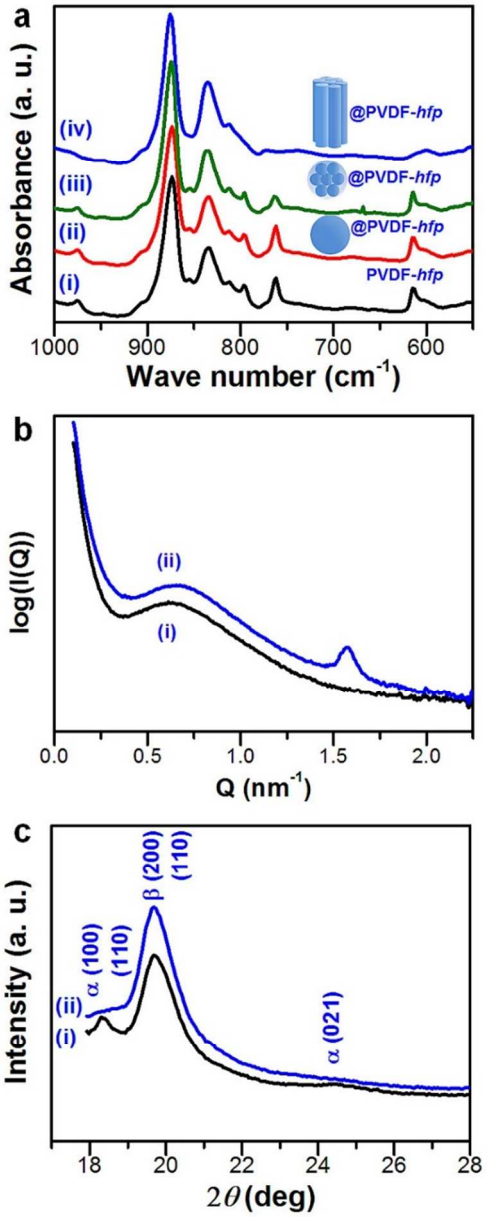

Fig. 2 (a) FTIR-ATR spectra of (i) PVDF-*hfp* reference and the nanocomposites by (ii) SiO_2, (iii) *m*-SiO_2 nanospheres, and (iv) *m*-SiO_2 nanorods; (b) SAXS and (C) *in situ* WAXS patterns for (i) PVDF-*hfp* and (ii) *m*-SiO_2 nanorod@PVDF-*hfp*, where the peak at Q=$4\pi sin\theta/\lambda$=1.58 nm^{-1} corresponds to (100) hexagonal ordered arrays in the mesoporous nanorods.

It is well known that PVDF-*hfp* consists of periodic crystalline lamellar stacks.[30] SAXS pattern reveals an increase of interlamellar spacing (determined by $L = 2\pi/Q_{max}$) from 6.9 nm to 7.5 nm with the *m*-SiO_2 nanorods (Fig. 2c). Hence, besides entire β phase formation, an effectively enhanced lamellar ordering for PVDF-*hfp* was achieved with the nanorods. In addition, the crystallite size associated with β (200)(110) was estimated to be ~ 15.7 nm by Scherrer equation from the WAXD pattern. Based on above, the crystalline lamellar structure of the *m*-SiO_2 nanorod@PVDF-*hfp* can thus be viewed in Fig. S3a.

To evaluate the efficiency of our approach, concentration effects of *m*-SiO_2 nanorods on the β phase formation were investigated (Fig. 3), where the weight percentages of the nanorods were quanfitied by thermogravimetric analysis (TGA) (Fig. S4). The dominance of β phase is prevailing in all the FTIR-ATR and XRD spectra. Though weak diffraction signal attributed to α(110) can still be detected with 4.3 wt% nanorods, complete β phase formation was achieved above 6.5 wt% nanorods. It is therefore an efficient method of incorporating *m*-SiO_2 nanorods to achieve β-PVDF-*hfp*.

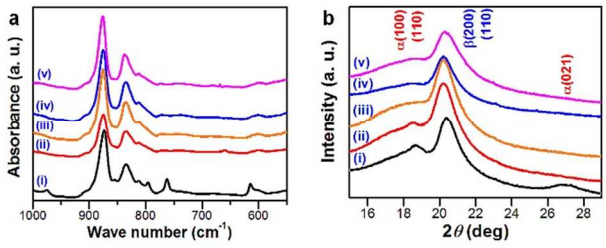

Fig. 3 (a) FTIR-ATR and (b) XRD stduy of the concentration effects on β phase formation by *m*-SiO_2 nanorods of (i) 0 wt%, (ii) 4.3 wt%, (iii) 6.5 wt%, (iv) 17.2 wt%, and (v) 34.4 wt%, respectively.

Piezo-/Ferro-electric properties

PFM amplitude signals in Fig. 4a clearly revealed the ferroelectric domains under an ac signal for the synthesized *m*-SiO_2 nanorod@PVDF-*hfp* in the absence of sample poling and stretching. Also, the *m*-SiO_2 nanorod@PVDF-*hfp* showed greatly enhanced nominal polarization comparing to the PVDF-*hfp* reference. This electroactive behavior may not be due to intrinsic ferroelectric polarization, which is possibly due to dielectric loss under large field.[31,32]

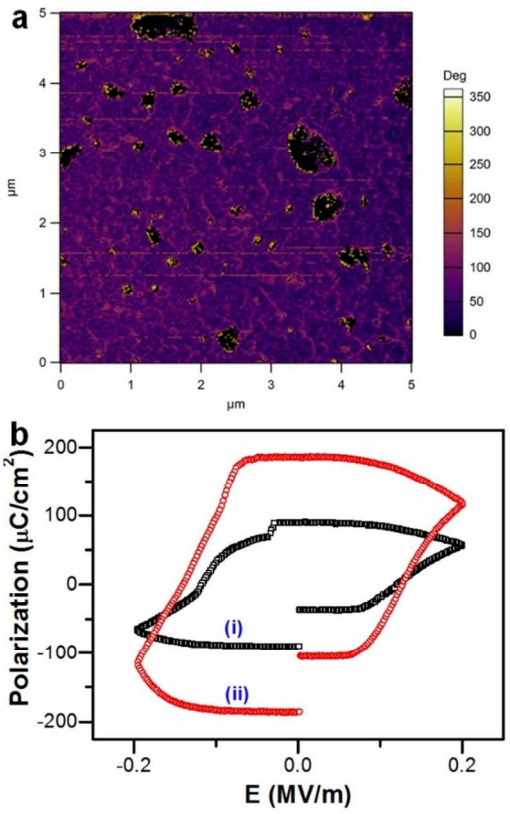

Fig. 4 (a) PFM phase image of *m*-SiO_2 nanorod@PVDF-*hfp*; (b) Polarization loops for the (i) PVDF-*hfp* and (ii) *m*-SiO_2 nanorod@PVDF-*hfp*.

Morphology

Columnar-like domains were observed by FESEM for both of the PVDF-*hfp* and *m*-SiO_2 nanorod@PVDF-*hfp* (Fig. S5a and 5a). Interestingly, round-shape like contrast rather than rod-shape were present through top view regarding the film gemotery. This may reasonably represent the short-axis planes of the nanorods. High magnification image (Fig. 5b) differentiates individually dispersed fillers and a larger portion of aggregated fillers whose dimensions correspond to ~ 2-4 times of short-axis diameter of the nanorod. TEM image provides further insight into these aggregates formed by an approximate side-by-side assembling cluster of the nanorods (Fig. 5c). Such arrangement is representative during TEM sampling (see also Fig. 5d for the view of a cluster along the long-axis of the nanorods) that is further confirmed by cross section SEM (Fig. S5b). The microstructure revealed by FESEM and TEM suggests: (1) the clustering of the *m*-SiO_2 nanorods may be energetic preferential during film growth, (2) together with crystalline phase identification, the nanorods, either in cluster form or individual form, promote the growth of *β*-PVDF-*hfp*, and (3) the alignment of short-axis plane of the nanorod and basal plane of the columnar-like domain is likely due to the interfacial interaction.

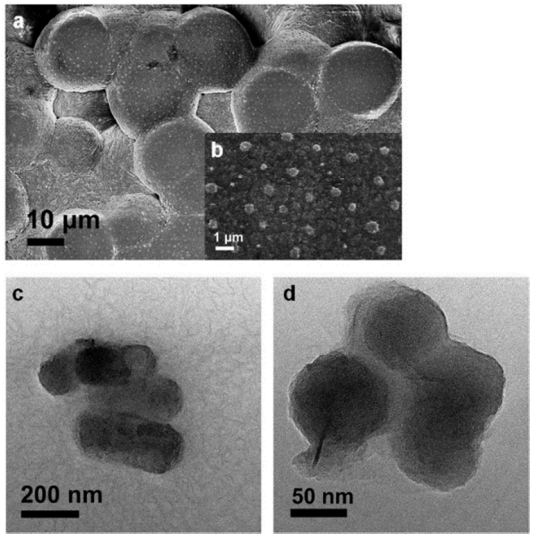

Fig. 5 (a) FESEM image of *m*-SiO_2 nanorod@PVDF-*hfp* with (b) high magnification image showing the disperison of the nanorods; (c, d) TEM image of *m*-SiO_2 nanorod@PVDF-*hfp*.

Formation mechanism: hydrogen bonding

We further investigated the interfacial interaction between the *m*-SiO_2 nanorods and PVDF-*hfp* matrix. The FTIR-ATR spectra for –OH groups (~ 3750-2500 cm^{-1}) are shown in Fig. 6. Trace amount of absorbed –OH was detected for the PVDF-*hfp* reference, which can be understood by its hydrophobic nature. Comparison on spectra tells the absorption features at 3444 and 3242 cm^{-1} were introduced by the nanorods. Features at 3414 and 3338 cm^{-1} emerged with 4.3 wt% nanorods, which can be considered to be the red-shift of –OH groups due to hydrogen bond formation.[23,25] With increase of the *m*-SiO_2 content to 34.4 wt%, the emerging vibrational features became even more broadened. It is difficult to differentiate any further peak shift from the strongly overlapped spectroscopic features. Annealing was applied to reduce the contribution from loosely bonded –OH towards the overlapped features, like surface absorbed –OH. Through annealing, the relative intensity of the surface –OH decreased relative to the emerging one, e.g., the intensity ratio of 3444 to 3338 cm^{-1} decreased from 0.99 to 0.95. Such better thermal stability of emerging –OH is consistent with its bonded nature. Though above indicates indirectly the presence of hydrogen bonding, broad IR absorption features hinder shedding light on the bond formation.

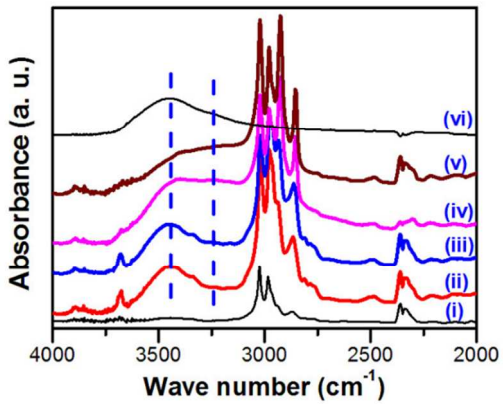

Fig. 6 FTIR-ATR spectra concerning –OH absorption for *m*-SiO_2 nanorod contents of (i) 0 wt%, (ii) 4.3 wt%, (iii) 17.2 wt%, (iv) and (v) 34.4 wt% and 34.4 wt% with annealing, with (vi) *m*-SiO_2 nanorod as reference.

Assume a hydrogen bond of –OH···FC– forms, corresponding shift of binding energies (BEs) for C and O is expected with electron transfer from $F^{\delta-}$ to $H^{\delta+}$.[33-36] To gain the insight to bonding information, we analyzed the XPS spectra of the *m*-SiO_2 nanorod@PVDF-*hfp* samples (Fig. 7). Elemental scan on C*1s* allows identification of $–CF_3$, $-CF_2$, -CF, -CO, $-CH_2$, and C-H/C-C species.[37,38] Gaussian fitting was applied to deconvolute the XPS spectra (See example for the PVDF-*hfp* reference in Fig. S6a). It shows that the C*1s* BEs of the carbonfluorine species exhibit a blue-shift with the addition of *m*-SiO_2 nanorods. This blue-shift was enlarged with increasing content of the nanorods, which reached 0.22, 0.23, and 0.16 eV for $–CF_3$, $-CF_2$, and –CF respectively at the nanorod content of 34.4 wt% (Table S1). On the other hand, –OH contribution was extracted from O*1s* spectra. The deconvolution of the broad O*1s* band tells a red-shift for the emerging –OH with reference to the absorbed –OH (Table S2, see also Fig. S6b for the fitting). This red-shift was 0.84 eV for 17.2wt% nanorods. With 34.4 wt% nanorods, the emerging –OH further red-shifted by 1.04 eV and possessed 56.4% of the total –OH content. A correlated blue-shift of C*1s* and red-shift of O*1s* was then found in the *m*-SiO_2 nanorod@PVDF-*hfp*, which is the experimental proof to the hydrogen bond formation. Therefore, our study provides the direct evidence of hydrogen bond formation for the long-proposed –OH···FC– system.

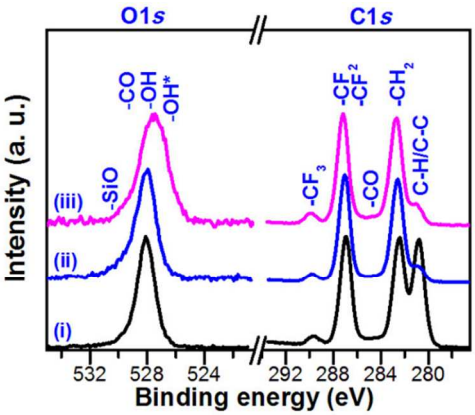

Fig. 7 XPS spectra of C1*s* and O1*s* for *m*-SiO_2 nanorod contents of (i) 0 wt%, (ii) 17.2 wt%, and (iii) 34.4 wt% show a corresponding blue-shift of C1*s* and red-shift of O1*s*.

Formation mechanism: arrangment of surface groups

Recent studies, i.e., successful β phase formation by anodic alumina membrane template with well-defined –OH and negligible enhancement on β phase by SiO_2 nanoparticles, suggest that besides desirable hydrogen bonding, arrangement of –OH groups is critical for the polar molecular conformation of PVDF-*hfp*. To examine our hypothesis on the arrangement of –OH, two more types of SiO_2 nanostructures, nanospheres (~ 100 nm) and mesoporous nanospheres (~ 105 nm), were applied to PVDF-*hfp* (Fig. S7). In both cases, α and β phases co-existed at filler 17.2 wt% content (Fig. 2a). The relative β fractions (F(β)s) can be semi-quantified based on a well-established empirical relation:

$$F(\beta) = A_\beta/(1.26A_\alpha + A_\beta),$$

where A_β and A_α are the measured absorbance values at 836 and 763 cm^{-1} individually, and 1.26 is the ratio of absorption coefficients for pure β and α phases at the respective wave numbers.[17,21,39] The F(β) increased from 0.57 for SiO_2 nanospheres@PVDF-*hfp* to 0.69 for *m*-SiO_2 nanosphere@PVDF-*hfp*. No appreciable change in the F(β) value can be seen comparing the SiO_2 nanospheres@PVDF-*hfp* to PVDF-*hfp*, which is consistent with the literature. The increase of F(β) by *m*-SiO_2 nanospheres then indicates promoting effects from internally organized hexagonal arrays of mesopores with a pore size of ~ 3.2 nm. It is likely to be analogous to the confinement effect from the template.[22,24] Meanwhile, much higher BET surface area of *m*-SiO_2 comparing to its solid counterpart provides enriched –OH sites for hydrogen bonding (see Fig. S8 for the estimated –OH concentrations). Further, advantageous β phase formation by *m*-SiO_2 nanorods than their spherical counterparts indicates directly a shape factor. To this concern, we draw the highlihgt here: growth of β-PVDF-*hfp* is faciliated via nanostructures (in the form of substrate or template) endowed with 1D (rod/tube) or 2D (planar) geometry through the arrangement of surface groups (e.g., –OH). Through arranged bonding sites, phase conformation can extend beyond local ordering. It can now be understood that radial intermolecular interaction surrounding SiO_2 nanosphere may not be able to retain the polar conformation in long range order with competing entropy. However, the anisotropic rod shape in our study is able to induce the polar conformation beyond the local ordering, thus leading to the entire formation of β phase. Our hypothesis is supported by the reported cases: (1) nearly spherical Ag and $BaTiO_3$ can not improve the β phase formation, (2) multi-wall CNT promotes the β phase growth even before post-processing, and (3) graphene induces γ phase formation.[13,19,20,40,41] Hence, both of the shape and mesopores of *m*-SiO_2 nanorods benefit the β phase conformation in our synthetic design.

We further apply fluoroalkyl modified *m*-SiO_2 nanostructures to β phase formation of PVDF-*hfp*. Two facts are noted in Fig. S9:–CF_3 modified nanorods also lead to entire β-PVDF-*hfp*; the nanorods again show advantage than their spherical counterparts in the phase formation. Since hydrophobic interaction may operate in the above example, it demonstrates an extention of the arrangement approach towards a wider intermolecular interaction regime other than the hydrogen bond focused in this work.

Conclusions

In summary, we have developed an easy and efficient method to synthesize β-PVDF-*hfp* film via incorporating *m*-SiO_2 nanorods. The use of *m*-SiO_2 nanorods has the merits of anisotropic shape and organized mesopores that direct polar molecular conformation towards oriented growth of β-PVDF-*hfp* and meanwhile improve the lamellar ordering. Through XPS analysis, direct evidence of hydrogen bond formation for the –OH···FC– system is provided for the first time in PVDF system. Besides anchoring intermolecular interaction, an arragnment of –OH groups is essential to induce oriented ordering of molecular conformation towards long range order. Our proposed mechanism could be used to explain unambiguously the existing controversy in current literature reports for the β-PVDF/-PVDF-*hfp*

formation. Futher, we demonstrated that this arrangement of surface functional group approach can be easily extended for the growth of *β*-PVDF-*hfp* with a variety of intermolecular interactions, which largely benefits current development in PVDF-/PVDF copolymer-based electroactive devices.

Notes and references

[a] *Department of Materials Science and Engineering, National University of Singapore, 7 Engineering Drive 1, Singapore, 117574*
[b] *Institute of Materials Research and Engineering, 3 Research Link, Singapore, 117602*
* msehc@nus.edu.sg

† Electronic Supplementary Information (ESI) available: FTIR of *m*-SiO_2 nanorods, DSC, TGA, HRSEM, TEM characterizations, polarization loops measurement, analysis of SAXS data, and fitting of XPS spectra of *m*-SiO_2 nanorod@PVDF-*hfp*; TEM images of SiO_2 and *m*-SiO_2 nanoparticles; FTIR of *m*-SiO_2-F17. See DOI: 10.1039/b000000x/

††Acknowledgement: We appreciate Dr. Guo Rui for the PFM study. We acknowledge Fan Zhen for the discussion on the polarization-electric field hysteresis loops and Tang Tao for the discussion on molecular conformation.

††† The authors would like to acknowledge the financial support from SERC to National University of Singapore under grant number 1123004036.

1 A. J. Lovinger, *Science*, 1983, **220**, 1115.
2 P. Ueberschlag, *Sensor Rev.*, 2001, **21**, 118.
3 P. C. A. Hammes and P. P. L. Regtien, *Sensor Actuator A*, 1992, **32**, 396.
4 A. K. Tripathi, A. J. J. M. van Breemen, J. Shen, Q. Gao, M. G. Ivan, K. E. Reimann, R. Meinders and G. H. Gelinck, *Adv. Mater.*, 2001, **23**, 4146.
5 M. Lee, C. Chen, S. Wang, S. N. Cha, Y. J. Park, J. M. Kim, L. Chou, and Z. L. Wang, *Adv. Mater.*, 2012, **24**, 1759.
6 X. Zhang, X. Huang, C. Li, and H. Jiang, *Adv. Mater.*, 2013, **25**, 4093.
7 J. Lee, K. Y. Lee, M. K. Gupta, T. Y. Kim, D. Lee, J. Oh, C. Ryu, W. J.Yoo, C. Kang, S. Yoon, J. Yoo and S. Kim, *Adv. Mater.*, 2014, **26**, 765.
8 R. Hasegawa, Y. Takahashi, Y. Chatani and H. Tadokoro, *Polym. J.*, 1972, **3**, 600.
9 Y. Takahashi and H. Tadokoro, *Macromolecules*, 1980, **13**, 1317.
10 M. Kobayashi, K. Tashiro and H. Tadokoro, *Macromolecules*, 1975, **8**, 158.
11 P. Martins, A. C. Lopes and S. Lanceros-Mendez, *Prog. Polym. Sci.*, 2014, **39**, 683.
12 G. H. Kim, S. M. Hong and Y. Seo, *Phys. Chem. Chem. Phys.*, 2009, **11**, 10506.
13 Y. Ahn, J. Y. Lim, S. M. Hong, J. Lee, J. Ha, H. J. Choi and Y. Seo, *J. Phys. Chem. C*, 2013, **117**, 11791.
14 R. Gregorio and D. S. Borges, *Polymer* 2008, **49**, 4009.
15 X. Tian, X. Jiang, B. Zhu and Y. Xu, *J. Membr. Sci.*, 2006, **279**, 479.
16 Y. Wu and S. L. Hsu, *J. Phys. Chem. B*, 2012, **116**, 7379.
17 C. Liang, Z. Mai, Q. Xie, R. Bao, W. Yang, B. Xie and M. Yang, *J. Phys. Chem. C*, 2014, **118**, 9104.
18 A. Anson-Casaos, J. M. Gonzalez-Dominguez, A. M. Diez-Pascual, M. A. Gomez-Fatou and M. T. Martinez, *J. Phys. Chem. C*, 2012, **116**, 16127.
19 S. Yu, W. Zheng, W. Yu, Y. Zhang, Q. Jiang and Z. Zhao, *Macromolecules*, 2009, **42**, 8870.
20 L. Gao, J. He, J. Hu and Y. Li, *J. Phys. Chem. C*, 2014, **118**, 831.
21 P. Martins, C. Caparros, R. Goncalves, P. M. Martins, M. Benelmekki, G. Botelho and S. Lanceros-Mendez, *J. Phys. Chem. C*, 2012, **116**, 15790.
22 V. Cauda, B. Toree, A. Falqui, G. Canavese, S. Stassi, T. Bein and M. Pizzi, *Chem. Mater.*, 2012, **24**, 4215.
23 X. Li, Y. Lim, K. Yao, F. E. H. Tay and K. H. Seah, *Chem. Mater.*, 2013, **25**, 524.
24 V. Cauda, S. Stassi, K. Bejtka and G. Canavese, *ACS Appl. Mater. Interfaces*, 2013, **5**, 6430.
25 S. Chen, K. Yao, F. E. H. Tay and C. L. Liow, *J. Appl. Phys.*, 2007, **102**, 104108.
26 J. Park, Y. Seo, I. Kim and C. Ha, *Macromolecules*, 2004, **37**, 429.
27 J. Kim, W. Cho and C. Ha, *J. Polym. Sci., Part B: Polym. Phys.*, 2002, **40**, 19.
28 C. Tsai, Y. Hung, Y. Chou, D. Huang, J. Hsiao, C. Chang, Y. Chen and C. Mou, *Small*, 2008, **4**, 186.
29 T. Yu, A. Malugin and H. Ghandehari, *ACS Nano*, 2011, **5**, 5717.
30 D. Lin, C. Lin and S. Guo, *Macromolecules*, 2012, **45**, 8824.
31 L. Pintilie and M. Alexe, *App. Phys. Lett.*, 2005, **87**, 112903.
32 H. Kliem and B. Martin, *J. Phys: Condens. Matter*, 2008, **20**, 321001.
33 H. R. Crabtree, P. E. M. Siegbahn, O. Eisenstein, A. L. Rheingold and T. F. Koetzle, *Acc. Chem. Res.*, 1996, **29**, 348.
34 G. A. Jeffrey, An Introduction to Hydrogen Bonding; Topic in Physical Chemistry, Oxford University Press, New York, 1997.
35 S. Zhou, X. Zheng, X. Yu, J. Wang, J. Weng, X. Li, B. Feng and M. Yin, *Chem. Mater.*, 2007, **19**, 247.
36 J. Xu, C. B. He, K. C. Toh and X. Lu, *Macromolecules*, 2002, **35**, 8846.
37 C. Yao, Li, X.; Neoh, K. G.; Shi, Z. and Kang, E. T. Appl. Surf. Sci. 2009, **25**, 3854-3858.
38 S. Mitra, A. Ghanbari-Siahkali, P. Kingshott, K. Almdal, H. K. Rehmeier and A. G. Christensen, *Polym. Degrad. Stab.*, 2004, **83**, 195.
39 R. JR. Gregorio and M. Cestari, *J. Polym. Sci., Part B: Polym. Phys.*, 1994, **32**, 859.
40 D. W. Chae and S. M. Hong, *J. Polym. Sci., Part B: Polym. Phys.*, 2010, **49**, 2379.
41 L. Zhang, D. Zha, T. Du, S. Mei, Z. Shi and Z. Jin, *Langmuir*, 2011, **27**, 8943.